Phosphorylation Facilitates the Integrin Binding of Filamin under Force

Harvey S. Chen, Kevin S. Kolahi, and Mohammad R. K. Mofrad*
Molecular Cell Biomechanics Laboratory, Department of Bioengineering, University of California, Berkeley, California

ABSTRACT Filamins are actin binding proteins that contribute to cytoskeletal integrity and biochemical scaffolds during mechanochemical signal transductions. Structurally, human filamins are dimers composed of an actin-binding domain with 24 immunoglobulin (Ig)-like repeats. In this study, we focus on the recently solved high-resolution crystal structure of Ig-like repeats 19–21 of filamin-A (IgFLNa-R19–R21). IgFLNa-R19–21 is of marked importance because it contains the binding site for integrins and facilitates the dynamic ability of filamin-A to communicate with the extracellular environment. However, the structure of filamin-A shows an interesting domain arrangement where the integrin binding site on IgFLNa-R21 is hindered sterically by IgFLNa-R20. Thus, a number of hypotheses on the regulation of filamin-A exist. Using molecular dynamics simulations we evaluated the effects of two primary regulators of filamin-A, force and phosphorylation. We find that a tensile force of 40 pN is sufficient to initiate the partial removal of the autoinhibition on the integrin binding site of IgFLNa-R21. Force coupled to phosphorylation at Ser^{2152}, however, affords complete dissociation of autoinhibition with a decreased force requirement. Phosphorylation seems to decrease the threshold for removing the IgFLNa-R20 β-strand inhibitor within 300 ps with 40 pN tensile force. Furthermore, the molecular dynamic trajectories illustrate phosphorylation of Ser^{2152} without force is insufficient to remove autoinhibition. We believe the results of this study implicate filamin-A as a tunable mechanosensor, where its sensitivity can be modulated by the degree of phosphorylation.

INTRODUCTION

The dynamic nature of the cytoskeleton is due, in part, to the multitudes of reorganizing proteins that alter the geometry of the cytoskeletal network. Consequentially, as the geometry of the cytoskeleton is altered, so are the physical characteristics of the cell such as, shape, position, stiffness, and even metabolism (1,2). It was once believed that cells lacked major organization and that their cytosol was likened to a soup of chemicals. However, recent evidence is surfacing that illustrate a precise localization of signal transduction and intracellular biochemistry. This is made possible by the precise organization of cellular factors that are either directly or indirectly anchored to the cytoskeleton. In addition to this scaffolding role that the cytoskeleton plays during signaling and metabolism, the cytoskeleton itself can also serve as a transducer of mechanical stimuli through cascades involving second messengers that are actin-associated proteins (3–6).

Of these actin-binding proteins, filamin plays an important dual role in regulating the dynamic integrity of the actin cytoskeleton and in cellular mechanotransduction. Filamins contain the unique capacity to orient the actin filaments orthogonally resulting in the formation of a 90° meshlike F-actin network (7). Filamins function as molecular dimers, and are classically described as functioning in formation of lamellipodia, but are also localized to the cortical actin network to function as a scaffold for a trafficking transmembrane receptors, signaling and adaptor proteins (1,2,7). In addition to functioning as an actin-binding protein, filamin can be degraded by proteolysis yielding products that may function as signaling molecules, integrating nuclear and cytosolic pathways (8–10).

Of the three existing homologs, filamin-A is most abundant and widely expressed (7,11) and is essential to normal human development (12,13). The diversity in phenotypes associated with different filamin mutations shows that filamins carry out a variety of essential functions and the current evidence suggests that in many cases specific disease phenotypes will result from disruption of specific interactions between IgFLNa-R domains and their binding partners (14).

Each human filamin-A (FLNa) monomer is a 240–280 kDa actin cross-linking protein composed of an N-terminal actin-binding domain, a rod domain of 24 immunoglobulin (Ig)-like repeats (IgFLNa-R) (Fig. 1 *A*) (7,15,16). Electron microscopy and sequence analysis studies suggest a v-shaped structure for filamin due to hinges between IgFLNa-R15 and -R16 and IgFLNa-R23 and -R24 (17,18). More recently, however, IgFLNa-R domain 19–21 (IgFLNa-R19–21) was crystallized, and an unexpected domain arrangement was discovered that illustrated IgFLNa-R20 as partially unfolded and brings IgFLNa-R21 into close proximity to IgLFNa-R19 (14). The N-terminus of IgFLNa-R20 forms a β-strand that associates with IgFLNa-R21, which has been identified previously as a major binding site for integrin adhesion receptors (14,19–21) (Fig. 1 *B*). This β-strand sterically hinders the binding of IgFLNa-R21 to integrin adhesion receptors (14).

The major role of filamin-A and integrin binding is to regulate cell spreading and survival (22). Other research has shown that filamin-A may modulate cell sensitivity to force and mechanoprotection (23,24). Integrin $\alpha\beta$-heterodimers

Submitted November 21, 2008, and accepted for publication August 17, 2009.

Harvey S. Chen and Kevin S. Kolahi contributed equally to this work.

*Correspondence: mofrad@berkeley.edu

Editor: Reinhard Lipowsky.

0006-3495/09/12/3095/10 $2.00

doi: 10.1016/j.bpj.2009.08.059

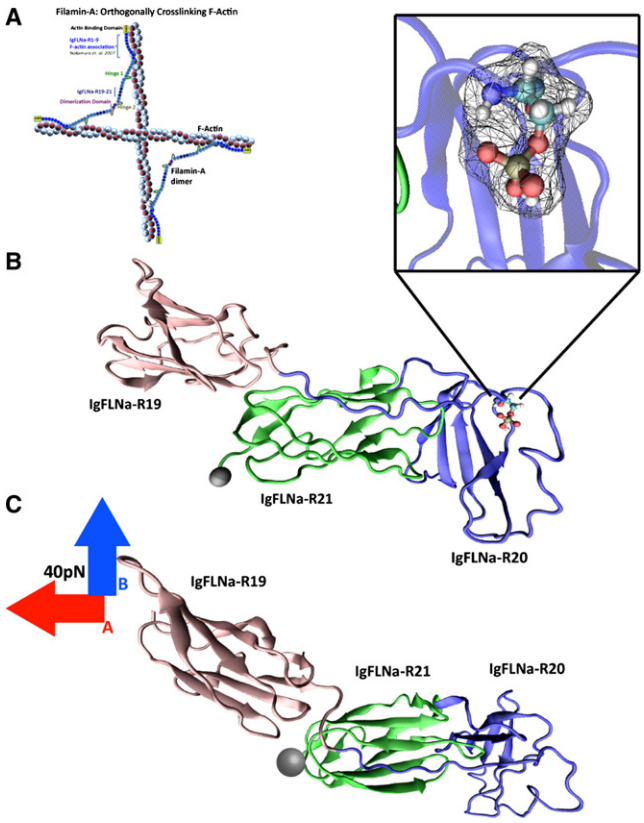

FIGURE 1 (*A*) Illustration of the structure of a human filamin-A. The figure also illustrates how filamins crosslinks actin filaments into orthogonal networks in cortical cytoplasm. At the N-terminus is the actin binding domain, and is followed by the Ig-like repeats (IgFLNA-R1–IgFLNA-R24). This study focuses on the binding of integrin with filamin-A at rod repeat 21. (*B*) The structure of IgFLNa-R19–21 with Ser-^{2152} phosphorylation illustrated (*circled*). IgFLNa-R19 is on the left; IgFLNa-R20 is on the right; IgFLNa-R21 is in the middle. The phosphoSer^{2152} residue was shown circled. The protein structure was obtained through Protein Data Bank (PDB ID: 2JS3) (14), and the Ser^{2152} side chain was modified through CHARMm software. (*C*) A depiction of how the tension force was applied to the unphosphorylated rod domain repeats 19–21, Model 4. In these simulations, the C-terminus of repeat 21 was fixed, which is represented by a gray bead. In *A*, force was applied to pull the N-terminus of repeat 19 along the axis of the rod domain. We also tested the effect of torque as in *B*. With torque the autoinhibition could be further removed from the integrin bind site of repeat 21.

that span the plasma membrane connect the extracellular environment to the actin cytoskeleton (5,8). Thus, the filamin-integrin complexes could provide a mechanical and biochemical link through which the actin cytoskeleton could respond to external cues. Filamin-A binds integrin at IgFLNa-R21, and leads to the transduction of mechanical stimuli from extracellular domain to intracellular domain through focal adhesions (25).

The structure of IgFLNa-R21 is a β-sandwich composed of two β-sheets. The integrin β7 cytoplasmic domain binds to the CD face of the IgFLNa-R21 (26). The CD face is the integrin-binding site formed by the two β-strands that were identified by a previous study (26). In our model, the CD face corresponds to the two β-strands formed by amino acid residues 2268–2287. Integrin binding to IgFLNa-R21 can be inhibited by phosphorylation of the integrin tail or by other integrin tail binding proteins that compete with filamin (14). NMR and biochemical analyses indicate that the IgFLNa-R20-21 domain pair inhibits integrin β-tail binding and mutations perturbing the IgFLNa-R20-21 interaction enhance integrin binding (27).

It has been suggested that disrupting this IgFLNa-R20 and IgFLNa-R21 interaction will reveal the binding site for integrin on IgFLNa-R21 and facilitate the binding to integrin. Three methods of regulation have been proposed, mechanical force, phosphorylation of the inhibitory domain on Ser^{2152} residue, and alternative splicing leading to splicozymes lacking the inhibitory peptide region (14,19–21). In addition, these three hypotheses may be seemingly interrelated. For example, mechanical signals are abundant in cell biology and are intimately linked with biochemical signaling pathways (28,29).

The objective of this study is to test the hypotheses leading to the activation and integrin binding of filamin-A. It has been illustrated previously that lack of the inhibitory region through alternative splicing increases the interaction of filamin with integrin (11,30). The inhibitory domain of IgFLNa-R20 regulates the filamin-A integrin-binding on IgFLNa-R21. This study focuses on the phosphorylation of Ser^{2152} and the applied mechanical force, which are two important potential factors involved in regulating integrin binding. Functionally, forces applied to this region can physically dissociate the inhibitory domain of IgFLNa-R20, but this may be independent and exclusive of phosphorylation at this same site. Alternatively, the two mechanisms, phosphorylation and mechanical force, may work synergistically, and these questions motivate our experimental endeavor.

MATERIALS AND METHODS

Crystal structure of IgFLNa-R19–21 was obtained through Protein Data Bank (PDB ID: 2JS3) (14). A complete filamin molecule, including all 24 rod domain IgFLNa-Rs has not yet been crystallized successfully. Visual molecular dynamic (MD) software was used to explore the secondary structure of the protein and for postprocessing of our MD results (31).

The simulated structure corresponds to the amino acid residues 2045–2329 of the full length filamin-A sequence. The atomistic coordinates for residues 2163–2170 and 2191–2197 were undetermined in the original published IgFLNa-R19–21 structure (14). The missing structure was completed using structural and sequence alignment methods with SWISS-MODEL-EXPASY software (14,32–34). The missing residues corresponded to isolated loop-like regions of IgFLNa-R21.

MD simulations were carried out using software CHARMm version c32b1 (35,36). CHARMm was also used to model the phosphate group onto Ser^{2152} (Fig. 1 *B*) (36). A switching function with values between 12.0 Å and 13.0 Å were used to cut off with nonbonding van der Waals and electrostatic interactions. The total number of atoms within the system was 4195 and 4199 for unphosphorylated and phosphorylated models, respectively. The models were linearly heated to 310 K and constant steering forces of 0–40 pN were applied for 5 ns (37). However, all the noticeable conformation changes occurred within the first 500 ps. After the 500 ps

time frame, all the models showed stabled conformations as determined through root mean-square deviation (RMSD) calculations of the α-carbon backbone. Therefore, we decided to discuss the model within the 500 ps timescale.

To represent solvent environment, an implicit model was used for solvent-protein interactions, namely the analytical continuum electrostatics (ACE) water model available in CHARMm (38). This model approximates the electrostatic and nonelectrostatic contributions of water molecules to the effective free energy. Poisson's equation was used to calculate the electrostatic contribution to the free energy (38). The ACE parameters were set to 1.0 IEPS (dielectric constant used for the space occupied by the molecule), 80 SEPS (dielectric constant used to approximate solvent), ALPHA 1.3 (Gaussian density distribution that determines atom volume), and sigma 2.5 (hydrophobic contribution scaling value to ACE).

The implicit water model simulates aqueous environment by treating the water molecules as a continuum dielectric constant while incorporating the free energy change due to solvation (39). After the implicit models, we confirmed all our simulations using the explicit model for water representation as well (40). When a water molecule makes a hydrogen bond (h-bond) with the protein backbone, its lifetime can be longer than several picoseconds (41). This can lead to cooperative dissociation of the backbone h-bond network. In implicit solvent simulations, even if a h-bond is temporarily destabilized, it will soon reform because the solvation effect is implemented as smooth energy surface so that the H and O atoms are still in a local energy well.

The implicit model was always preferred initially because in explicit models the large number of water molecules yield intractable within reasonable timeframes. Furthermore, modeling the solvent explicitly is exceptionally computationally demanding, as the number of atoms can increase at least an order of magnitude. It was necessary to limit our use of explicit water simulations as a reference and validation tool only, rather than an explorative one.

Six simulation models were used to study the effect of tension force and phosphorylation, and the parameters used are summarized in Table 1. We simulated all possible combinations of phosphorylation and force. Models including force are pre-equilibrated, or in other words are continuations of models 1 and 2. For each simulation, a constant force was applied to the N-terminal residue on IgFLNa-R19 with the magnitudes of force for each simulation of Model 3 to 6 were 10,20,30, and 40pN of force. In addition, each scenario was repeated a minimum of five times to verify the observed trajectories.

To determine a relevant order of magnitude of tension force to remove the autoinhibitory strand, a constant velocity model in explicit water box was run using NAMD. The model was phosphorylated, and the constraints and direction of pull followed exactly as the models they were representing (Table 1). The velocity was 0.0002 Å/ps, and the model was run for 50 ns over a 100 Å distance. The resulting force required was ~100 pN. Therefore, we decided to use 10 pN with 10 pN increment to begin the experiment.

Constraints applied in the MD simulations and justifications

Initially, to test for the effect of phosphorylation and forces, only the C-terminus on IgFLNa-R21 was fixed. However, with only the C-terminus (Pro^{2328}) fixed, the repeat containing integrin binding capacity, IgFLNa-R21, would unfold significantly at forces >20 pN (Fig. 2 *A*). This took place in both phosphorylated and nonphosphorylated models. Furthermore, the autoinhibition could not be dissociated before unfolding of IgFLNa-R21, and IgFLNa-R20 does not refold and approach the β-inhibitor as expected (see Results). Therefore, more constraints were added to IgFLNa-R21 to stabilize IgFLNa-R21. We empirically fixed residues on the C-terminal loop regions to stabilize IgFLNa-R21. Through minimizing these constraints we were able to identify residues that must be fixed to stabilize IgFLNa-R21 during tension, and the constraints used are summarized in Table 1. Consistently, we found residues Pro^{2328}, Pro^{2302}, and Pro^{2252} are necessary for stabilization of IgFLNa-R21 under tension (Fig. S1 in the Supporting Material). The *cis*-amide bond formed by proline produces a kink in the amino acid primary structure and from our analyses seems essential to maintain the Ig fold of IgFLNa-R21.

These constraints could also represent interactions that may exist in the full-length protein between the rod domain repeats IgFLNa-R20–21 and IgFLNa-R22–24. These interactions may stabilize IgFLNa-R20 and 21 when tension force is exerted and prevents significant conformational distortion during tension, preserving the integrin binding capability. Using multiple constraints also promoted the refolding of IgFLNa-R20, and in essence provides an interesting mechanistic hypothesis to the stabilization present once this autoinhibitory region is dissociated.

The direction of the mechanical perturbation was varied to identify the conformational reaction of the rod domain with torque applied, in addition to the axial tension (Fig. 1 *C* (*A*, *red arrow*)). After the MD simulation, the structural trajectories were analyzed to determine the conformational changes due to applied mechanical perturbations. Each IgFLNa-R is colored uniquely to clarify the relative movements of the repeats as well as the changes in structure (Fig. 1 *B*). The structural trajectories of the β-strand inhibitor were examined during the course of these simulations.

To assess the integrin binding characteristics of filamin-A, we assumed that the propensity of filamin to bind to integrin is increased when the β-strand inhibitor of IgFLNa-R20 has completely dissociated from the IgFLNa-R21, exposing the integrin binding site. We also consider that reassociation of the partially unfolded IgFLNa-R20 with its β-strand may also promote the stability of this potentially activated conformation of filamin-A.

RESULTS

In this study, we simulate hypothetical mechanisms of the activation of filamin-A integrin binding, namely phosphorylation of Ser^{2152} and mechanical force. The goal of these

TABLE 1 Models used in the simulations

Model	Phosphorylation on Ser^{2152}	Force applied on IgFLNa-R19	Constraints (protein residue No.)	Implicit model system size (atoms)	Explicit model system size (atoms)	Maximum duration of simulation (10^{-9} s)
1	No	n/a	2328	4195	62,104	5.0
2	Yes	n/a	2328	4199	62,187	5.0
3	No	40 pN	2328 or 2302 or 2252–2255 or 2278–2281	4195	330,468	5.0
4	Yes	40 pN	2328	4199	332,516	5.0
5	Yes	40 pN	2328 or 2302 or 2252–2255 or 2278–2281	4199	332,516	5.0
6	No	50 pN	2328 or 2302 or 2252–2255 or 2278–2281	4199	330,468	5.0

Model 1 served as the control, where no force or phosphorylation occurred, and confirms the crystallographic structure determined by Lad et al. (14). Model 2 included only physiological phosphorylation, and no force. Model 3 tests only the effect of force on this rod region. Model 4 and 5 test force and phosphorylation together. Constraints are required when force is applied to this rod region to stabilize the integrin binding site. Model 6 illustrates that 50 pN of force was needed to remove autoinhibition when phosphorylation is not present. n/a is defined as having no force applied.

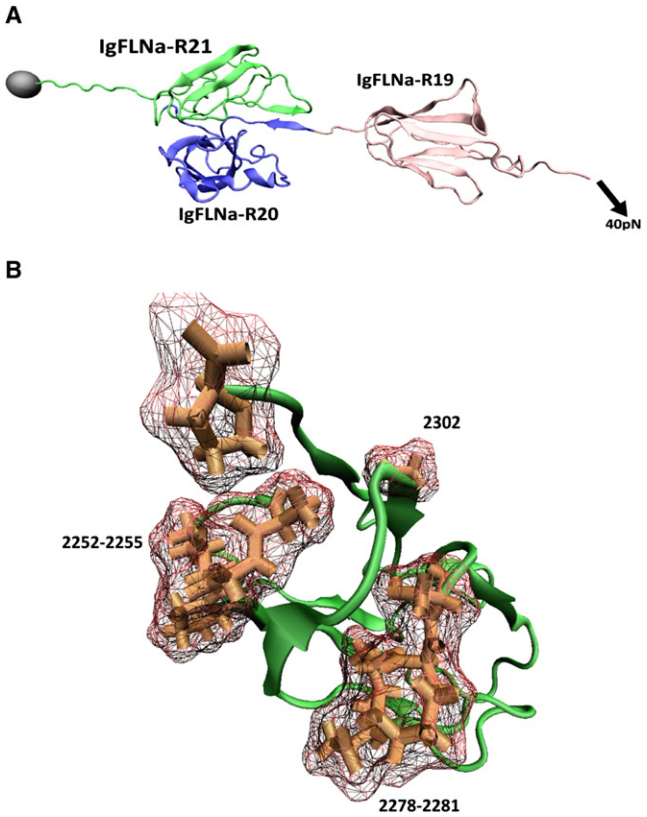

FIGURE 2 (*A*) Result of Model 4. FLNa-R21 was deformed due to only fixing one amino acid in the C terminus. FLNa-R21 deformation was undesirable and may be the reason why the β-inhibitor was not removed in this case. The β-inhibitor was less likely to leave FLNa-R21 when FLNa-R21 was deformed. (*B*) An illustration of the positions of the multiple stabilizing constraints on repeat 21. Of these 10 amino acids, four of them (2328, 2302, 2255, and 2278) are proline. By stabilizing these C-terminal loops of repeat 21, the structure was increasingly stable during tension and did not linearize under tension (Fig. 3 *A*).

simulations is to identify if Ser^{2152} phosphorylation or mechanical force-induced activation of the integrin binding of filamin-A are possible. However, how phosphorylation or force can mechanistically accomplish this is unknown.

In this study, all combinations of phosphorylation and tension total are tested, the absence of tension and phosphorylation of Ser^{2152}, our negative control, a phosphorylated Ser^{2152} model without tension, an unphosphorylated Ser^{2152} model with tension, and a combination of phosphorylation of Ser^{2152} and tension. As our simulations of these models proceeded, it became necessary to include a fifth model to further test and explore the effects of the loading conditions imposed, and additional simulations with greater forces, 50 pN, and timescales, 5.0 ns, were also carried out. In the following result descriptions, please keep in mind that the force magnitudes quoted are used for relative comparisons and may not necessarily reflect the magnitudes of force experienced by filamin-A under physiological conditions, i.e., they can be considerably smaller in vivo.

Model 1: without force and phosphorylation, the autoinhibition cannot be removed

Model 1 was the negative control without phosphorylation or applied force. The model was run with the complete IgFLNa-R19–21 rod region. This simulation did not illustrate any propensity of conformational change within 5 ns of simulation run. The explicit solvent models also expressed no conformational change. Six simulations all illustrate that the crystallized structure of IgFLNa-R19–21 determined by Lad et al. (14) was indeed a stable conformation at physiological conditions in the absence of force and phosphorylation (Fig. 1 *C* (*A*, *red arrow*)). In Model 1, the average RMSD over the whole trajectory for 5 ns was 4.455 Å, with a standard deviation of 0.464 Å. The RMSD value was consistent during simulations at ~20 ps (Fig. S2).

Model 2: without force applied but with phosphorylated Ser^{2152}, the autoinhibition still cannot be removed

Model 2 was a phosphorylated control that did not include external force application. Surprisingly, the result was the same as in Model 1; we had anticipated that phosphorylation would alter the conformation of this region to affect autoinhibition. Extending the simulation time beyond 500 ps to 5 ns did not show any potential conformational changes due solely to phosphorylation. Despite the increased ionic character with the added phosphoryl group, our simulations with explicit solvent models also confirmed the lack of a meaningful conformational change (Fig. 1 *B*). This puts into question whether or not activation can take place in the absence of any physical forces.

In Model 2, the average RMSD over the whole trajectory for 5 ns was 5.573 Å, and the standard deviation was 0.237 Å. The RMSD value does not fluctuate significantly beyond the 40 ps timepoint (Fig. S2).

Model 3: without phosphorylation and pulled under 40 pN, the autoinhibition began to dissociate, yet complete removal cannot be achieved

Model 3 was devised to test the effect of force only. In contrast to Models 1 and 2, force can drastically alter the conformation of the model (Fig. 3 *A*). The model was pulled for a total of 5 ns under 40 pN. After 100 ps of simulation, dissociation of the β-strand inhibitor does not occur and the integrin binding site fails to become exposed (Fig. 3 *A*). No further conformational change takes place in the following time.

Furthermore, a shearing force is exhibited during the β-strand's association with the integrin binding site of IgFLNa-R21. This can be visualized by the distortion in the CD-face of IgFLNa-R21 (Fig. 3 *A*). Despite increasing the force even beyond the typical 40 pN, the β-strand inhibitor fails to dissociate before IgFLNa-R21 loses significant

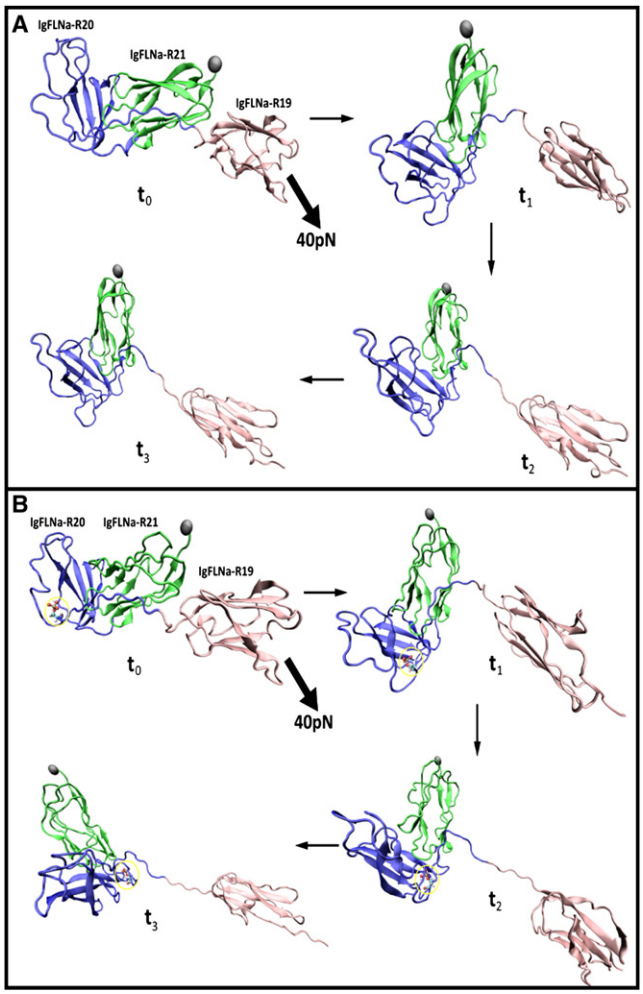

FIGURE 3 (*A*) Molecular trajectory of filamin-A rod domain repeats 19–21 under 40 pN of tension, Model 3, is illustrated. Multiple stabilizing constraints were applied in this model. Each arrow represents ~100 ps. At t1, or ~100 ps, the center of mass of repeat 19 (*right*) translates away to move away from the center of mass of repeat 21 (*middle*). The gray bead represents the harmonic constraint on repeat 21. Although torque and tension is being applied to the β-strand inhibitor of IgFLNa-R20, the force is not sufficient to result in complete dissociation of the β-strand inhibitor and the integrin binding site of repeat 21. The autoinhibition remained bound through the end of the simulation, t3, and even if the simulation proceeded to 1ns. (*B*) The filamin-A rod region 19–21 under tension with phosphoryl modification of Ser^{2152}, Model 5, is illustrated here. The gray bead represents the harmonic constraint on the C-terminus of the rod domain. With the phosphorylation of Ser^{2152} residue, further dissociation from the integrin binding site of the inhibitor is apparent within 100 ps. With 40 pN and after 300 ps, the inhibition begins to further dissociate and translate away from the integrin-binding site, and alternatively associates with repeat 20. Within 500 ps with 40 pN tension, the β-inhibitor can be removed completely.

tertiary structure even with many stabilizing constraints imposed. The intramolecular forces between the β-strand of IgFLNa-R20 and IgFLNa-R21 can however tolerate tensions >40 pN.

During initial simulations, force was applied parallel to the axis of the rod domain, to result in pure tension without any resulting bending moment. However, tensile forces applied parallel to the rod domain axis and β-strand inhibitor fail to offer a component of force that will abduct the β-strand inhibitor from IgFLNa-R21. This inevitably underlies the observation that the β-strand inhibitor appears to shear the CD-face of IgFLNa-R21, and fails to dissociate (Fig. 3 *A*). This is a consequence of the inherent geometry and conformation of the rod domain. We therefore hypothesized that autoinhibition could be removed by pulling the bound β-strand inhibitor from IgFLNa-R20 normal to the plane containing the CD-face, exerting a torque in addition to tension (Fig. 1 *C* (*B*, *blue arrow*)).

Whereas the application of torque leads to partial dissociation of the inhibitory β-strand (Fig. 3 *A*), the complete dissociation could not be achieved due to IgFLNa-R21 loss of tertiary structure under tension. Further partial removal could be achieved through stabilizing constraints described in Materials and Methods. We note the salt bridge between Arg^{2146} and Asp^{2287} is significant enough to resist complete dissociation of the autoinhibition. The result of this study implied that bending of the rod domain is essential in the removal of the autoinhibition in unphosphorylated models (Fig. 3 *A*).

Model 4: IgFLNa-R21 unfolded into linear sequence with only the C-terminus residue fixed, but the partial removal of autoinhibition may suggest that the phosphorylation lowers the constraint requirement

This model was first set to test the effect of phosphorylation and external forces. Initially, we imposed no stabilizing constraints for IgFLNa-R21. Although deformation of the C-terminal domain of IgFLNa-R21 does occur with a 40 pN tensile force, partial removal comparable to Model 3 could be obtained with decreased magnitude of force as compared to Model 3, e.g., with 30 pN (Fig. 3 *A*). Despite the deformation that occurs in the N-terminal domain of IgFLNa-R21 at 30 pN of tension force, the autoinhibitory β-strand can be partially removed, but the association of Arg^{2146} with Asp^{2287} seemed to be limiting. This removal is analogous to the case in which a 40 pN force is applied as in Model 3, and can result in partial removal of inhibition as illustrated in Fig. 3 *A*. Complete dissociation of the β-strand is prevented by the ionic interaction between Arg^{2146} with Asp^{2287} as in Model 3.

These results are surprising because partial removal could not be accomplished in Model 3 without larger magnitude of force and stabilizing constraints on IgFLNa-R21. This translates to a change in the requirements for the removal of the inhibitory β-strand, and therefore the autoinhibition seemed more likely to dissociate with phosphorylation present at Ser^{2152}.

Moreover, IgFLNa-R20 showed a tendency to refold at 100 ps with a 30 pN force applied, and despite autoinhibition

persisting. By this refolding we mean that IgFLNa-R20 appeared to rotate and position its anti-parallel β-strand sandwich such that the inhibitory β-strand could position and associate in an anti-parallel manner (Fig. 3 *A* and Fig. 4 *B*). However, we note again that the destabilization of tertiary structure of IgFLNa-R21 when subject to applied force is an unrealistic and undesired phenomenon. Therefore, constraints were required to maintain the stability of IgFLNa-R21, and were implemented in Model 5.

Model 5: with phosphorylation and applied 40 pN, the autoinhibition was successfully removed within 500 ps

Model 5 involved multiple constraints. Through trial and error, the constraints were set as shown in Table 1. Residues within the exposed loops near the C terminus of IgFLNa-R21 were harmonically constrained, and the number of constraints was reduced to a minimum that could necessitate maintenance of stability of IgFLNa-R21 during tension. All of the fixed amino acids resided in IgFLNa-R21, and were primarily proline residues, or adjacent to proline residues. The fixed residues on IgFLNa-R21 are shown in Fig. 2 *B*. Of the 10 fixed amino acids shown in Table 1, four of them were prolines, namely residues 2328, 2302, 2255, and 2278. The other six residues were all neighboring prolines that helped to stabilize the proline turns.

Using these extra constraints was justifiable as prolines are unique amino acid residues that often provide kinks and turns in the tertiary structure of proteins. These proline residues provide the turns between the β-pleated sheets in all repeats in filamin-A. Therefore, fixing these prolines stabilizes IgFLNa-R21 by maintaining the tertiary structure of IgFLNa-R21 and preventing the hydrogen bonds between the β-pleated sheets from being disrupted by tension. Although the model only includes IgFLNa-R19, -R20, and -R21, it was suspected that IgFLNa-R22 or even further repeats may provide stabilizing interaction with IgFLNa-R21. In vivo, repeats IgFLNa-R22–24 may interact with the proline residues and prevent IgFLNa-R21 from unfolding on application of force. Unfortunately, this hypothesis cannot be tested at this moment because IgFLNa-R19–21 is the most complete elucidated crystal structure of filamin-A, and these interactions should be probed if a structure becomes available. Model 5 illustrates clear dissociation of the autoinhibition. In the first 100 ps, similar to Model 3, the IgFLNa-R19 center of mass begins to move away from the center of mass of IgFLNa-R21. However in contrast to Model 3, at ~300 ps, IgFLNa-R20 begins to rotate and orient itself in an antiparallel fashion as it increases its proximity to the β-strand inhibitor. At 350 ps, the autoinhibition completely dissociates from IgFLNa-R21, and thus integrin binding is no longer sterically hindered (Fig. 3 *B*) (see Movie S1). The dissociated β-strand that was inhibiting the integrin binding of IgFLNa-R21 begins to alternatively associate with its native tandem repeat, IgFLNa-R20 (see Movie S1). This interaction seemed to stabilize and hold the dissociated β-strand inhibitor in place, and only occurs with phosphorylation.

In contrast to Model 3, pure tension without any torque is sufficient to drive dissociation of the β-strand inhibitor. With a 40 pN force, the direction of pulling appeared unimportant, and all cases resulted in complete removal of auto inhibition within 500 ps, analogous to the trajectory of Fig. 3 *B*.

An interesting observation was that the phosphorylated Ser^{2152} residue laid within this non-β-pleated sheet amino acid loop (Fig. S1). Moreover, this amino acid loop appeared to have a strong tendency to fold toward the β-strand inhibitor in IgFLNa-R20. The simulation showed that during the refolding of IgFLNa-R20, the loop and β-pleated sheet migrate toward each other (see Movie S1). Taking a closer look at the residues of the amino acid loop and the β-strand inhibitor, there were four consecutive arginine residues upstream of the inhibitor. The positively charged arginine residues have relatively high affinity for the negatively charged phosphate group on Ser^{2152}.

Model 6: without phosphorylation, 50 pN is required to remove autoinhibition

Model 6 was set out to test the minimum force required to remove the autoinhibition in nonphosphorylated model. The trajectory was similar to that of Model 5, which showed complete removal of the autoinhibition within 100 ps.

Smaller forces applied to Model 3 and 5 did not remove autoinhibition completely

Further simulations were carried out to test for the minimum force required to remove the autoinhibition. Models pulled with 10 pN and 20 pN did not propose appreciable conformational changes in the protein. The center of mass of IgFLNa-R19 did not translate away from IgFLNa-R21 (data not shown), and IgFLNa-R20 did not show any refolding tendency. On the other hand, when 30 pN of tension is applied, the distance of center of masses of IgFLNa-R19 and IgFLNa-R21 does increase, and IgFLNa-R20 began to appear to refold, apparently rotating to position the bound β-strand inhibitor into an anti-parallel β-strand topology, all within 100 ps. A partial dissociation of the β-strand inhibitor, where Arg^{2146} remains bound, could be accomplished within 400 ps with phosphorylation. However, extending this 30 pN tension simulation to 5 ns did not illustrate that a complete removal is possible with 30 pN(data not shown). This test implies that a minimum force of 40 pN is required to remove autoinhibition.

Explicit solvent models agreed with implicit models

We tested Models 3–6 by running simulations that incorporated an explicit water box model to represent the solvent

interactions more explicitly. During the first 100 ps we were able to simulate, the trajectory was identical to the result in our implicit model—the distance of the center of masses of IgFLNa-R19 and IgFLNa-R21 increased with a 40 pN force, the β-strand inhibitor began to dissociate similarly, and IgFLNa-R20 appeared to associate with the previously bound β-strand inhibitor. The molecular trajectories in both explicit and implicit models were analogous in both phosphorylated and nonphosphorylated models.

DISCUSSIONS

The integrin binding activation of filamin-A is hypothesized to occur through three potential mechanisms, by phosphorylation at Ser^{2152}, mechanical force, or alternative splicing generated isoforms of filamin-A. Although alternative splicing is not tested in this study, our results can shed light on two of the three current hypotheses leading to filamin-A integrin binding activation. Activation of filamin-A's integrin binding capacity is evaluated by determining if autoinhibition is disrupted and the integrin binding site of IgFLNa-R21 is exposed. Testing the combined effects of tension on IgFLNa-R19-21 and phosphorylation revealed that phosphorylation of Ser^{2152} without tension is not sufficient to result in activation. However, by increasing the applied force, the β-strand inhibitor from IgFLNa-R21 without phosphorylation can be removed. The results suggest that the phosphorylation is there to decrease the requirement, and thus increase the chance, to remove the autoinhibition. Removal of autoinhibition can still be achieved without phosphorylation. Physiologically, integrin binding of filamin-A may be activated after being phosphorylated at Ser^{2152} and when subsequent tension is applied to the rod domain.

Phosphorylation was also shown to lower the constraints requirements, magnitude of force (or torque) required for complete removal of the β-strand inhibition of IgFLNa-R21. This conclusion was derived by comparing the trajectory events in Models 2–6. Models 1–3 are controls. Model 1 was not phosphorylated and no force was applied. Model 2 was phosphorylated but not pulled, whereas Model 3 was pulled but not phosphorylated.

The results of Model 1 and 2 were interesting and unexpected. Without any applied pulling force, the structure showed no meaningful conformational changes. In a previous work by Lad et al. (14), mechanical force had been proposed as a possible regulatory mechanism for the promotion of filamin-A integrin binding. In addition, phosphorylation was also listed as a possible method to elicit filamin-A integrin binding, but is insufficient in modulating integrin binding activity in experiments (42). In our phosphorylation simulations, however, we found by comparing Models 2 and 1, where Model 2 was phosphorylated, and Model 1 unphosphorylated, that the results were identical. Neither model illustrated a tendency to dissociate the autoinhibition present on IgFLNa-R21. On the other hand, simulating force on an unphosphorylated IgFLNa-R19-R21, Model 3, autoinhibition could at least partially be removed with higher forces and with maximum torque, i.e., perpendicularly to the rod domain axis. We note that this event in Model 3 does require stabilization of IgFLNa-R21. Complete removal in a nonphosphorylated model requires more applied force than its phosphorylated counterpart.

Although Model 1 and 2 suggest that the integrin inhibitory strand does not dissociate from filamin-A without applied force, other experiments (42) support that filamin-A binds with integrins isolated from cell lysates, where there is assumed to be no applied force. To address this problem, we re-equilibrated Model 3 and 4 for 3 ns. After the integrin-binding site is exposed and tension removed, we observed no potential to refold. Thus, we hypothesize that the filamin-A was activated previously by force before the cell was lysed.

The geometry of the complex formed by β-strand inhibitor and IgFLNa-R21 CD face underlies why an absolute absence of torque cannot sufficiently accomplish removal of the autoinhibition. To drive dissociation of the β-strand inhibitor, a torque must be supplied. The β-strand inhibition sits within a groove formed on the CD face of IgFLNa-R21 by two antiparallel β-strands of this same repeat (Fig. 1 *B*). Pure tension simply results in a shear stress on the face of this groove and only serves to further destabilize the tertiary structure of IgFLNa-R21. An effective torque applies a component of force that serves to displace the β-strand from the binding site. Thus, the logical way to remove the inhibitor was to pull it away, in a direction perpendicular to and outward of the plane containing the three interacting β-strands (Fig. 1 *C*). We noted, however, that pure tension can result in dissociation of the β-strand when the rod region IgFLNa-R19-21 is phosphorylated at Ser^{2152}. This may be accomplished by the phosphoserine attraction with $Arg^{2146–2149}$. These strong interactions on the β-strand inhibitor may provide sufficient torque to allow removal of the β-strand inhibitor from the integrin binding site of IgFLNa-R21 during tension.

Phosphorylation increases effectively the sensitivity of removal of the autoinhibition of IgFLNa-R19–21 to loading conditions. Furthermore, the magnitude of tension could be reduced to result in filamin-A activation of integrin binding. Although phosphorylation of the Ser^{2152} residue lowers the threshold of tensile force required to remove the autoinhibition, we found that mechanical force was necessary to remove the autoinhibition and reveal the binding site for integrin. In other words, phosphorylation of Ser^{2152} without force is not sufficient to result in removal of the autoinhibition on IgFLNa-R21.

In the experiment by Travis et al. (42), phospho-blocking or mimicking mutations did not interfere with the ability of integrin-binding in cell lysate. This finding in light of our results, leads one to propose that the function of phosphorylation on Ser^{2152} is kinetic rather than thermodynamic. Phosphorylation reduces the force and constraints requirements,

increases the chance to remove autoinhibition, and thus causes the integrin binding reaction to proceed quicker. However, with sufficient force and time, the autoinhibition will eventually be removed. In the experiment by Travis et al. (42), the cells remain intact for 48 h before they are lysed, and this may sufficiently activate a detectable population of filamin-A molecules.

We also speculated that applied tensile forces would lead to the refolding of IgFLNa-R20, and assist in the removal of autoinhibition, but could only find evidence for refolding of IgFLNa-R20 in phosphorylated models with tension (Models 4 and 5). In these models, the amino acid loop that contained phosphoSer^{2152} in IgFLNa-R20 (Fig. S1) approaches the β-strand inhibitor and associates with Arg$^{2146–2149}$ on the inhibitor. Furthermore, association with IgFLNa-R20 can stabilize the β-strand inhibition and the energetic costs of dissociation from IgFLNa-R21 may be compensated by this phenomenon. This interaction may serve to further promote integrin binding on IgFLNa-R21 by keeping the dissociated competitive inhibitor away from its binding site. The conformational changes discussed in this study may mechanistically describe activation of filamin-A's integrin binding in vivo. However, future studies should actually assess whether forced dissociation of the inhibitory β-strand of IgFLNa-R20 is sufficient to lead to filamin-A binding to integrin in vivo.

The stability of IgFLNa-R21 was also a significant factor in our analysis and in determining if integrin binding is possible once the autoinhibition has been removed. We hypothesize that the stabilizing constraints possibly represent downstream repeats, IgFLNa-R22–24, that may interact with IgFLNa-R21. Empirically we found 10 amino acids that were key for stability of IgFLNa-R21, four proline residues, and the remaining six being neighbors of these and other proline residues (Fig. 2 *B*). These proline residues provided turns and loops in the Ig-like fold and had a major role in maintaining the tertiary structure of IgFLNa-R21. However, this hypothesis cannot be tested with our current methods as no crystallized model, including IgFLNa-R21 and IgFLNa-R22 for example, is available currently (2,14,37).

Alternatively, these interactions may be required for the timescales under which we implemented our analysis. A decreased force magnitude may be sufficient to remove autoinhibition if this occurred over the relatively much longer duration of a microsecond. Eventually, the time dependence in these trajectories may be assessed in the future as increased computational power becomes available to allow for much longer scale simulations (43). We expect that the responses described herein may have considerably decreased stress thresholds in vivo and this should be investigated through simulating smaller forces on the rod region over much greater timescales.

Comparison between Model 3 and 5 illustrates the dramatic effect phosphorylation of Ser^{2152} may have on stability of the β-strand inhibitor. Between these two models, all variables were held constant with the exception of the phosphoryl modification of Ser^{2152} for Model 5 versus Model 3 where the structure was simulated without phosphorylation. Without phosphorylation, a minimum of 40 pN of tensile force was required to result in only partial removal of the β-strand inhibitor, but many stabilizing constraints must be imposed and the tension must induce significant torque. Nevertheless, autoinhibition could be destabilized and nearly disabled with forces as small as 30 pN extension forces with phosphorylation of Ser^{2152}, but a 40 pN force most reliably and quickly removed inhibition completely. This result strongly suggested that the phosphate group effectively decreased the requirement to remove the autoinhibition, and facilitates integrin binding, which could lead to a mechanotransduction event.

Phosphorylation on Ser^{2152} increases the affinity of this now modified, negatively charged residue to ionically interact with the positively charged arginine residues on the β-strand inhibitor, Arg$^{2146–2149}$ (Fig. S1). We find this phosphoserine binds to and stabilizes the β-inhibitor once it dissociates from the binding site. The salt bridges formed between phosphoSer^{2152} and the Arg$^{2146–2149}$ may stabilize the unbound β-strand facilitating its removal. Therefore, without phosphorylation of Ser^{2152}, higher tensile forces were required to remove the β-inhibitor.

Although our results showed that 40 pN was the minimum force required to remove the β-inhibitor, again we consider that in vivo over much longer timescales, less force may be required. To save computation time, we typically pulled the protein for 500 ps, which is relatively short as most biological reactions take place in a timescale of microseconds (44,45). If the model was pulled for longer time, the required force could decrease, but our multiple short simulations are statistically relevant (46).

The results from the models are consistent with the hypothesis that phosphorylation of Ser^{2152} decreases the loading constraints required to remove autoinhibition. Functionally, from these data we hypothesize phosphorylation of Ser^{2152} increases the sensitivity of the rod region IgFLNa-R19–21 to tensile forces. If phosphorylation serves to lower the tension threshold required to remove autoinhibition of filamin-A binding to integrin, then cell sensitivity to stress can be modulated. Therefore, phosphorylation of filamin-A can play an interesting dual role in the mechanosensitivity of the cell. Conversely, previous experiments by Shifrin et al. (23) and Glogauer et al. (24) have shown that filamin-A is necessary to modulate cellular desensitization to force. Filamin-A may mediate cell survival during mechanical stress via dephosphorylation and therefore decreasing cell sensitivity to force (23,24). However, the possibility remains that in vivo filamin-A may solely function in its phosphorylated form, and that both tension and phosphorylation are required for physiological activity.

Furthermore, because mechanical force is involved in the promotion of integrin binding, filamin-A may have a

phenomenal function in cellular mechanotransduction pathway. Although a recently published structure illustrating that the other two rod regions resembling IgFLN-aR20–21, IgFLNa-R16–17, and IgFLNa-R18–19, lack phosphorylation regulatory sites, mechanical force may alter the observed packed domain arrangements (47). Mechanical stimulation may facilitate multiple conformational changes in the rod domain. For instance, many in vivo and in vitro observations demonstrate the propensity of cells to form focal adhesions with mechanical stimuli (6,25,48,49). Filamin-A may be involved in the formation of focal adhesions from the maturation of focal complexes (8). Because the cortical actin network is under tension due to myosin-II activity, filamin-A can be activated once localized in the cortical network and therefore bind to integrin (22).

CONCLUSION

The simulations in this study suggest that mechanical force may be a major and direct cause of autoinhibition removal. Phosphorylation on Ser^{2152} increases the possibility of removal by decreasing the force and constraints requirement. However, the proline constraints used in the simulation models are obtained through trial and error. Although we provide many hypothetical explanations and justifications, further investigations are indeed desired, especially the interaction between IgFLNa-R21 and IgFLNa-R22–R24 that helps the stabilization of the model.

Future experiments should also consider identifying if cells indeed can modulate their mechanosensitivity via filamin-A phosphorylation. We are currently working to include a more complete molecular picture of cellular mechanotransduction, and hope to include future simulations of structures with more filamin-A repeats, filamin homologs and other actin-binding proteins. In addition, in vitro AFM experiments with filamin-A can serve as a great comparison with the molecular conformations proposed here. These experiments may be beneficial in supporting a clearer picture of cellular mechanotransduction.

SUPPORTING MATERIAL

A movie and two figures are available at http://www.biophysj.org/biophysj/supplemental/S0006-3495(09)01514-8.

The authors thank Dr. D. Calderwood for helpful discussions and insight. Technical assistance from J. Golji, M. Chen, and other members of Molecular Cell Biomechanics Laboratory is gratefully acknowledged.

This work was supported by a generous grant from the National Science Foundation (CBET0829205).

REFERENCES

1. Feng, Y., and C. A. Walsh. 2004. The many faces of filamin: a versatile molecular scaffold for cell motility and signaling. *Nat. Cell Biol.* 6:1034–1038.
2. Popowicz, G., M. Schleicher, A. Noegel, and T. Holak. 2006. Filamins: promiscuous organizers of the cytoskeleton. *Trends Biochem. Sci.* 31:411–419.
3. Ingber, D. E. 2006. Cellular mechanotransduction: putting all the pieces together again. *FASEB J.* 20:811–827.
4. Janmey, P. A., and C. McCulloch. 2007. Cell mechanics: integrating cell responses to mechanical stimuli. *Annu. Rev. Biomed. Eng.* 9:1–34.
5. Kaazempur Mofrad, M. R., N. A. Abdul-Rahim, H. Karcher, P. J. Mack, B. Yap, et al. 2005. Exploring the molecular basis for mechanosensation, signal transduction, and cytoskeletal remodeling. *Acta Biomater.* 1:281–293.
6. Mofrad, M. R. K., and R. D. Kamm. 2009. Cellular Mechanotransduction. Cambridge University Press, New York.
7. Stossel, T. P., J. Condeelis, L. Cooley, J. H. Hartwig, A. Noegel, et al. 2001. Filamins as integrators of cell mechanics and signaling. *Nat. Rev. Mol. Cell Biol.* 2:138–145.
8. Campbell, I. 2008. Studies of focal adhesion assembly. *Biochem. Soc. Trans.* 36:263–266.
9. Pudas, R., T. R. Kiema, P. J. Butler, M. Stewart, and J. Ylänne. 2005. Structural basis for vertebrate filamin dimerization. *Structure.* 13: 111–119.
10. Uribe, R., and D. Jay. 2009. A review of actin binding proteins: new perspectives. *Mol. Biol. Rep.* 36:121–125.
11. van der Flier, A., and A. Sonnenberg. 2001. Structural and functional aspects of filamins. *Biochim. Biophys. Acta.* 1538:99–117.
12. Fox, J. W., E. D. Lamperti, Y. Z. Ekşioğlu, S. E. Hong, Y. Feng, et al. 1998. Mutations in filamin 1 prevent migration of cerebral cortical neurons in human periventricular heterotopia. *Neuron.* 21:1315–1325.
13. Kyndt, F., J. P. Gueffet, V. Probst, P. Jaafar, A. Legendre, et al. 2007. Mutations in the gene encoding filamin A as a cause for familial cardiac valvular dystrophy. *Circulation.* 115:40–49.
14. Lad, Y., T. Kiema, P. Jiang, O. Pentikäinen, C. Coles, et al. 2007. Structure of three tandem filamin domains reveals auto-inhibition of ligand binding. *EMBO J.* 26:3993–4004.
15. Gorlin, J. B., R. Yamin, S. Egan, M. Stewart, T. P. Stossel, et al. 1990. Human endothelial actin-binding protein (ABP-280, nonmuscle filamin): a molecular leaf spring. *J. Cell Biol.* 111:1089–1105.
16. Nakamura, F., T. Osborn, C. Hartemink, J. Hartwig, and T. Stossel. 2007. Structural basis of filamin A functions. *J. Cell Biol.* 179:1011–1025.
17. Hartwig, J. H., and T. P. Stossel. 1981. Structure of macrophage actin-binding protein molecules in solution and interacting with actin filaments. *J. Mol. Biol.* 145:563–581.
18. Sutoh, K., M. Iwane, F. Matsuzaki, M. Kikuchi, and A. Ikai. 1984. Isolation and characterization of a high molecular weight actin-binding protein from *Physarum polycephalum* plasmodia. *J. Cell Biol.* 98: 1611–1618.
19. Jay, D., E. J. García, J. E. Lara, M. A. Medina, and M. de la Luz Ibarra. 2000. Determination of a cAMP-dependent protein kinase phosphorylation site in the C-terminal region of human endothelial actin-binding protein. *Arch. Biochem. Biophys.* 377:80–84.
20. Vadlamudi, R. K., F. Li, L. Adam, D. Nguyen, Y. Ohta, et al. 2002. Filamin is essential in actin cytoskeletal assembly mediated by p21-activated kinase 1. *Nat. Cell Biol.* 4:681–690.
21. Woo, M. S., Y. Ohta, I. Rabinovitz, T. P. Stossel, and J. Blenis. 2004. Ribosomal S6 kinase (RSK) regulates phosphorylation of filamin A on an important regulatory site. *Mol. Cell. Biol.* 24:3025–3035.
22. Kim, H., A. Sengupta, M. Glogauer, and C. Mcculloch. 2008. Filamin A regulates cell spreading and survival via β1 integrins. *Exp. Cell Res.* 314:834–846.
23. Shifrin, Y., P. D. Arora, Y. Ohta, D. A. Calderwood, and C. A. McCulloch. 2009. The role of FilGAP-filamin A interactions in mechanoprotection. *Mol. Biol. Cell.* 20:1269–1279.
24. Glogauer, M., P. Arora, D. Chou, P. A. Janmey, G. P. Downey, et al. 1998. The role of actin-binding protein 280 in integrin-dependent mechanoprotection. *J. Biol. Chem.* 273:1689–1698.

25. Lee, S. E., S. Chunsrivirot, R. D. Kamm, and M. R. Mofrad. 2008. Molecular dynamics study of talin-vinculin binding. *Biophys. J.* 95:2027–2036.

26. Kiema, T., Y. Lad, P. Jiang, C. L. Oxley, M. Baldassarre, et al. 2006. The molecular basis of filamin binding to integrins and competition with talin. *Mol. Cell.* 21:337–347.

27. Calderwood, D. A., A. Huttenlocher, W. B. Kiosses, D. M. Rose, D. G. Woodside, et al. 2001. Increased filamin binding to beta-integrin cytoplasmic domains inhibits cell migration. *Nat. Cell Biol.* 3:1060–1068.

28. Golji, J., R. Collins, and M. R. Mofrad. 2009. Molecular mechanics of the alpha-actinin rod domain: bending, torsional, and extensional behavior. *PLOS Comput. Biol.* 5:e1000389.

29. Linke, W. A., and A. Grützner. 2008. Pulling single molecules of titin by AFM—recent advances and physiological implications. *Pflugers Arch.* 456:101–115.

30. van der Flier, A., I. Kuikman, D. Kramer, D. Geerts, M. Kreft, et al. 2002. Different splice variants of filamin-B affect myogenesis, subcellular distribution, and determine binding to integrin [beta] subunits. *J. Cell Biol.* 156:361–376.

31. Humphrey, W., A. Dalke, and K. Schulten. 1996. VMD: visual molecular dynamics. *J. Mol. Graph.* 14:33–38, 27–38.

32. Peitsch, M. C. 1996. ProMod and Swiss-Model: Internet-based tools for automated comparative protein modelling. *Biochem. Soc. Trans.* 24:274–279.

33. Peitsch, M. C., T. Schwede, and N. Guex. 2000. Automated protein modeling–the proteome in 3D. *Pharmacogenomics.* 1:257–266.

34. Schwede, T., J. Kopp, N. Guex, and M. C. Peitsch. 2003. SWISS-MODEL: an automated protein homology-modeling server. *Nucleic Acids Res.* 31:3381–3385.

35. Brooks, B., and M. Karplus. 1983. Harmonic dynamics of proteins: normal modes and fluctuations in bovine pancreatic trypsin inhibitor. *Proc. Natl. Acad. Sci. USA.* 80:6571–6575.

36. MacKerell, A. D., M. S. Sommer, and M. Karplus. 1995. pH dependence of binding reactions from free energy simulations and macroscopic continuum electrostatic calculations: application to 2′GMP/3′GMP binding to ribonuclease T1 and implications for catalysis. *J. Mol. Biol.* 247:774–807.

37. Kolahi, K. S., and M. R. Mofrad. 2008. Molecular mechanics of filamin's rod domain. *Biophys. J.* 94:1075–1083.

38. Schaefer, M., H. W. van Vlijmen, and M. Karplus. 1998. Electrostatic contributions to molecular free energies in solution. *Adv. Protein Chem.* 51:1–57.

39. Chen, J., C. L. Brooks, and J. Khandogin. 2008. Recent advances in implicit solvent-based methods for biomolecular simulations. *Curr. Opin. Struct. Biol.* 18:140–148.

40. Phillips, J. C., R. Braun, W. Wang, J. Gumbart, E. Tajkhorshid, et al. 2005. Scalable molecular dynamics with NAMD. *J. Comput. Chem.* 26:1781–1802.

41. Raiteri, P., A. Laio, and M. Parrinello. 2004. Correlations among hydrogen bonds in liquid water. *Phys. Rev. Lett.* 93:087801.

42. Travis, M. A., A. van der Flier, R. A. Kammerer, A. P. Mould, A. Sonnenberg, et al. 2004. Interaction of filamin A with the integrin beta 7 cytoplasmic domain: role of alternative splicing and phosphorylation. *FEBS Lett.* 569:185–190.

43. Freddolino, P. L., F. Liu, M. Gruebele, and K. Schulten. 2008. Ten-microsecond molecular dynamics simulation of a fast-folding WW domain. *Biophys. J.* 94:L75–L77.

44. Schwaiger, I., A. Kardinal, M. Schleicher, A. A. Noegel, and M. Rief. 2004. A mechanical unfolding intermediate in an actin-crosslinking protein. *Nat. Struct. Mol. Biol.* 11:81–85.

45. Schwaiger, I., M. Schleicher, A. A. Noegel, and M. Rief. 2005. The folding pathway of a fast-folding immunoglobulin domain revealed by single-molecule mechanical experiments. *EMBO Rep.* 6:46–51.

46. Monticelli, L., E. J. Sorin, D. P. Tieleman, and V. S. Pande. 2008. Molecular simulation of multistate peptide dynamics: a comparison between microsecond timescale. *J. Comput. Chem.* 29:1740–1752.

47. Heikkinen, O. K., S. Ruskamo, P. V. Konarev, D. I. Svergun, T. Iivanainen, et al. 2009. Atomic structures of two novel immunoglobulin-like domain-pairs in the actin cross-linking protein filamin. *Biol. Chem.* 284:25450–25458.

48. Bershadsky, A. D., N. Q. Balaban, and B. Geiger. 2003. Adhesion-dependent cell mechanosensitivity. *Annu. Rev. Cell Dev. Biol.* 19:677–695.

49. Nicolas, A., B. Geiger, and S. A. Safran. 2004. Cell mechanosensitivity controls the anisotropy of focal adhesions. *Proc. Natl. Acad. Sci. USA.* 101:12520–12525.